Journal of Non-Crystalline Solids 630 (2024) 122904

Contents lists available at ScienceDirect

Journal of Non-Crystalline Solids

journal homepage: www.elsevier.com/locate/jnoncrysol

Effect of copper oxide amount on non-isothermal crystallization kinetics of diphosphate glasses

Majda Khaldi [a], Yousf Islem Bourezg [a,b,*], Mohamed Kharroubi [a], Foudil Sahnoune [c], Messaoud Harfouche [d], Ahcen Keziz [c], Mostafa Maache [a], Lakhdar Gacem [e], Djamel Bradai [f]

[a] Physico-Chemistry of Materials and Environment Laboratory, Faculy of Exact Sciences and Informatics, University of Djelfa, PO Box 3117, Djelfa 17000, Algeria
[b] Faculty of Technology, University of M'sila, BP 166, M'sila 28000, Algeria
[c] Physics Department, Faculty of Sciences, University Mohamed Boudiaf of M'sila, M'sila 28000, Algeria
[d] Synchrotron-light for Experimental Science and Applications in the Middle East (SESAME), Allan 19252, Jordan
[e] Faculty of Sciences, Ziane Achour University of Djelfa, BP 3117, Djelfa 17000, Algeria
[f] Faculty of Physics, USTHB, BP 32, El Alia, Algiers 16111, Algeria

ARTICLE INFO

Keywords:
Diphosphate glass
Copper oxide
Crystallization kinetics
XRD
DTA

ABSTRACT

The present study investigates the thermal behavior and structural properties of $Na_2Cu_xZn_{1-x}P_2O_7$ ($x = 0$, 1 and 5 mol%) glasses. Differential thermal analysis (DTA) under non-isothermal conditions and X-ray diffraction (XRD) techniques were used to explore the effect of CuO amount on the crystallization kinetics of the glasses. The characteristic temperatures were used to calculate the activation energy, enthalpy, Gibbs free energy and entropy as well as morphological parameters. A correlation between the obtained results from these two techniques provides valuable information about the crystallization behavior of these glasses as well as the structural role played by the transition metal oxide. In the present glass system, CuO increased the characteristic temperatures and energies of activation and it acted as a structure modifier. Moreover, a bulk crystallization mechanism with different dimensional growth of crystals for non-doped and doped samples was obtained. The kinetic evolution was compared and confirmed using different methods.

1. Introduction

Until recent years, glass materials have significantly motivated the interest of researchers due to the wide range of their applications, such as in optoelectronics, optical switching devices, optical fibers, laser medium, etc. Among a variety of oxide glasses, phosphate glasses are the better choice for luminescent solar concentrators [1], bio-glasses or glass ceramics [2,3], ionic conductors [4], storage of nuclear waste [5] and pigments [6–8]. The most known of phosphate based-glasses, diphosphates crystal structures have attracted much attention in the last recent years. These glasses have as formula $X_2YP_2O_7$ where X is an alkaline cation ($X = K$, Na, and Li, etc.) and Y is a transition metal ion (Y = Co, Zn, Mn, Fe, Ni, Cu, Zn, etc.) [9–13].

The application range of these glasses is expanded by adding transition metal ions like cobalt, manganese, copper, etc. Several oxidation states of such transition elements are found within glass matrices, allowing a wider range of glass properties to be achieved [14–16]. On one hand, many studies were focused on the electric, dielectric and crystal structure properties of such glasses, like, $Na_2ZnP_2O_7$ [17,18], $K_2ZnP_2O_7$ [18,19] and $K_2NiP_2O_7$ [20]. On the other hand, numerous investigations have only been conducted on Na-P_2O_7 based-glasses doped with various chemical elements, including their preparation, crystal structure characterization, and other properties determination [21–26].

Few data about the crystallization phenomenon and related parameters of $Na_2ZnP_2O_7$ crystal structure glasses exist in the literature. Some works presented the thermal behavior of Na-Zn-P_2O_7 glass series [27–29], focusing only on the reaction's peak temperatures such as glass transition T_g and crystallization phenomenon T_c. A recent study conducted the investigation of crystallization kinetics for $Na_2ZnP_2O_7$ glass, where many thermodynamic characteristics were extracted, i.e. T_g, T_c, activation energy E_c and morphological parameters n and m [30]. By the authors opinion, there is no research focused on the thermodynamics of the crystallization process for copper-doped $Na_2ZnP_2O_7$ glasses.

* Corresponding author at: Physico-Chemistry of Materials and Environment Laboratory, Faculy of Exact Sciences and Informatics, University of Djelfa, PO Box 3117, Djelfa 17000, Algeria.
E-mail address: y.bourezg@univ-djelfa.dz (Y.I. Bourezg).

https://doi.org/10.1016/j.jnoncrysol.2024.122904
Received 14 November 2023; Received in revised form 21 February 2024; Accepted 24 February 2024

Table 1
Chemical composition of the prepared glass samples (mol%).

Glass	P_2O_7	ZnO	Na_2O	CuO
NZPO	50.00	25.00	25.00	00.00
NZPO/1Cu	50.00	24.75	25.00	00.25
NZPO/5Cu	50.00	23.75	25.00	01.25

Therefore, the present study was aimed at investigating the thermal crystallization characteristics of $Na_2ZnP_2O_7$ glass containing different molar amounts of copper-transition metal. A special emphasis was on extracting and analyzing the thermodynamic properties such as crystallization peak temperature T_c, activation energy E, enthalpy $\Delta H^{\#}$, Gibbs free energy $\Delta G^{\#}$, entropy $\Delta S^{\#}$ and mode of crystallization parameters *n* and *m*.

2. Materials and methods

Three phosphate glasses were prepared with a chemical composition of $Na_2Cu_xZn_{1-x}P_2O_7$ ($x = 0$, 1 and 5 mol%). The samples were labeled as NZPO, NZPO/1Cu and NZPO/5Cu according to the Cu mole fraction in the glass. Different powders were used, $NH_4H_2PO_4$ (≥ 99.5%, POCH), Na_2CO_3 (≥99.5%, Sigma-Aldrich), ZnO (≥ 99.5%, Riedel), $Cu(NO_3)_2$ and $6H_2O$ (≥ 99.9%, Sigma- Aldrich). The glasses were prepared via melting and quenching schemes as reported in our earlier works [30, 31]. Table 1 shows the oxides composition of samples in molar percent units. The preparation of non-doped and Cu-doped glass samples obeyed the chemical reactions shown in Eqs. (1) and (2), respectively.

$$ZnO + Na_2CO_3 + 2NH_4H_2PO_4 \rightarrow Na_2ZnP_2O_7 + 2NH_3^{\uparrow} + 3H_2O^{\uparrow} + CO_2^{\uparrow} \quad (1)$$

$$(1-x)ZnO + Na_2CO_3 + 2NH_4H_2PO_4 + xCu(NO_3)_2 \rightarrow Na_2Zn_{(1-x)}Cu_xP_2O_7 + 2(1+x)NH_3^{\uparrow} + 3(1-x)H_2O^{\uparrow} + CO_2^{\uparrow} + 4xO_2^{\uparrow} \quad (2)$$

Thermal scans were carried out on a LABSYS EVO DTA/DSC-TG SETARAM analyzer. About ~ 70 mg of each sample were put in a standard alumina crucible and scanned at five heating rates (15, 20, 25, 30 and 35 K min^{-1}), over a temperature range from room temperature to 873 K. An empty alumina crucible was used as reference.

Phase identification was analyzed on an XRD XPERT-Pro diffractometer with monochromatic Cu-K_α radiation, operating at 40 mA and 40 kV with a scan step of 0.02 °/s.

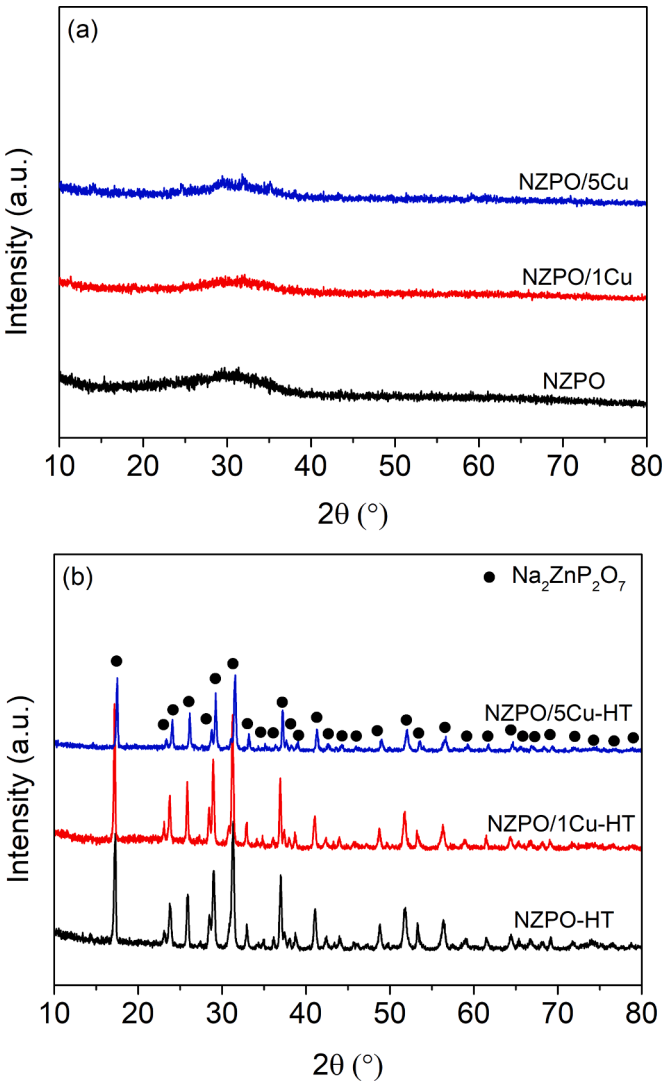

Fig. 2. X-ray diffraction patterns of as-prepared (a) and heat-treated (b) glass samples.

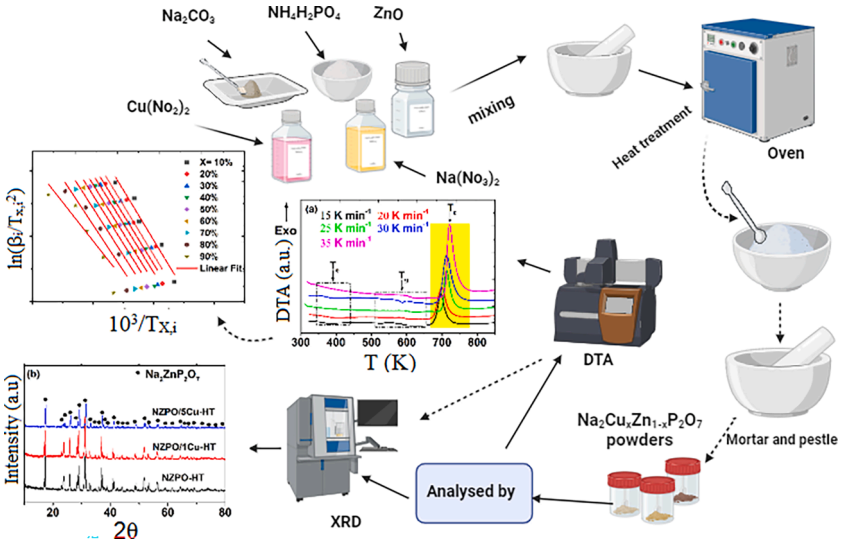

Fig. 1. Methodologies used in the present study for the preparation and characterization steps.

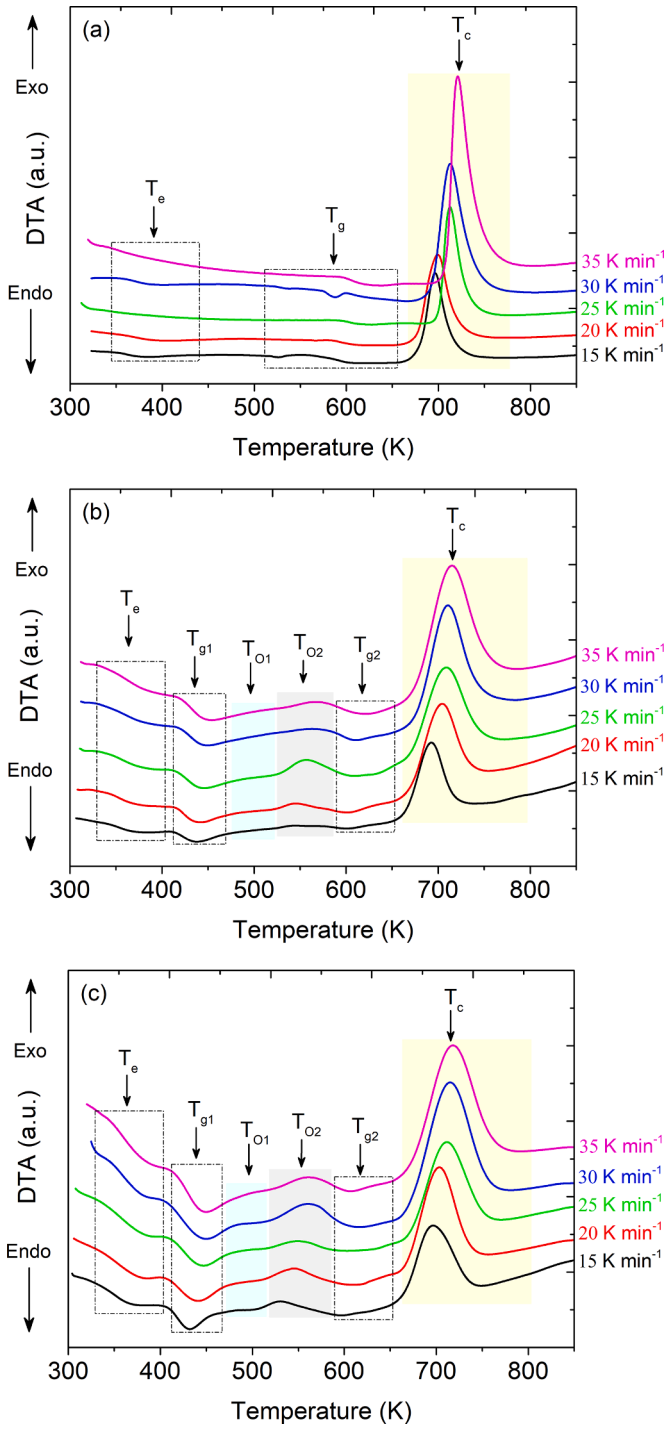

Fig. 3. DTA curves vs. temperature for no-doped (NZPO) (a) and Cu-doped NZPO glass samples, NZPO/1Cu (b) and NZPO/5Cu (c).

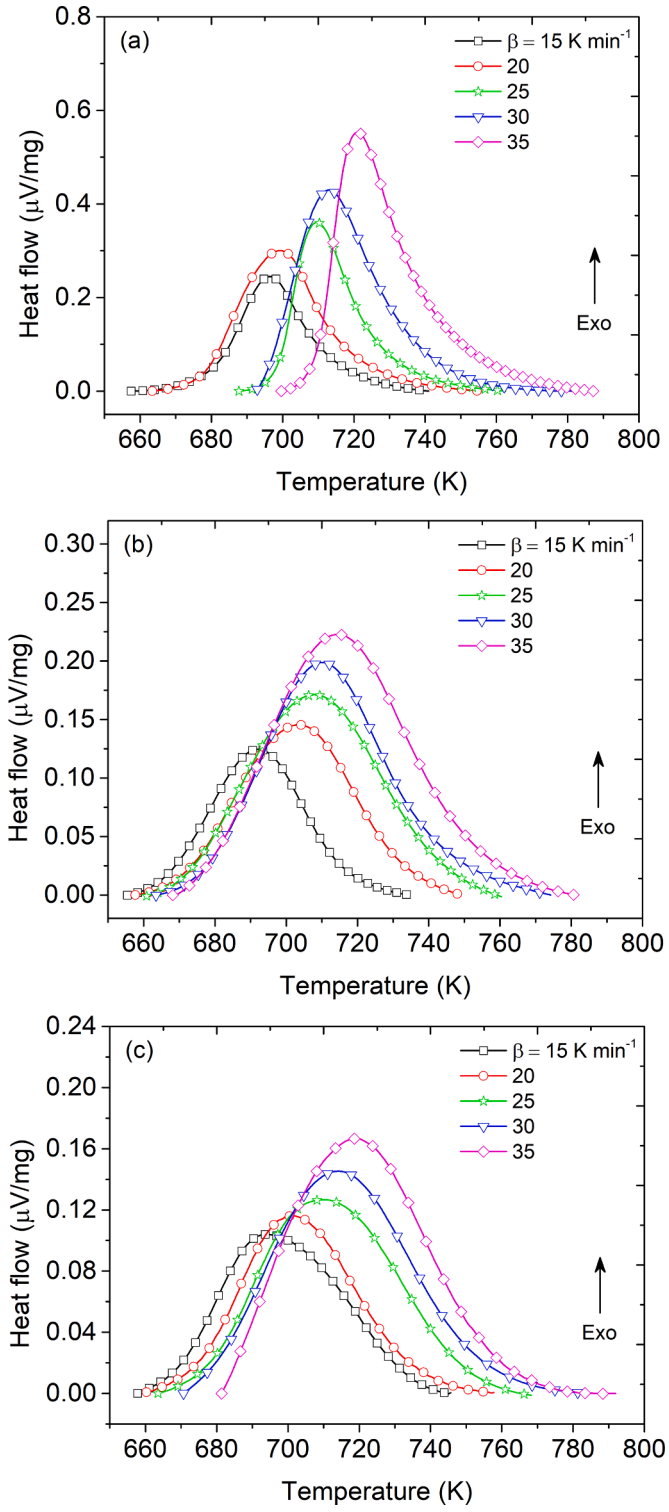

Fig. 4. Normalized crystallization peaks of (a) NZPO, (b) NZPO/1Cu and (c) NZPO/5Cu samples.

Fig. 1 summarizes the different preparation steps and characterization methodologies used in the present study.

3. Results and discusion

3.1. Characteristic temperatures

Fig. 2 shows the X-ray diffraction patterns for the as-prepared (Fig. 2a) and heat-treated samples (i.e. with symbol HT) at 923 K (Fig. 2b) of non-doped and Cu-doped NZPO glass samples up to 5 mol%. All the diffractograms of as-prepared states show the absence of diffraction lines, as shown in Fig. 2a. This is an indicative behavior of their amorphous glassy structure. However, the heat treated states NZPO-HT, NZPO/1Cu-HT and NZPO/5Cu-HT show the existence of sharp peaks proving that the glasses have been crystallized with a tetragonal structure $Na_2ZnP_2O_7$ (PDF 01–087–0499). This finding is in good agreement with the previous work for synthesized and heat treated NZPO glass [30]. No additional phase was observed in the Cu-doped samples. This means that the copper element occupies a substitutional

Table 2
Crystallization temperature characteristic for different glasses.

Sample	Peak temperature, T_C (K, ± 2 K)				
	15	20	25	30	35
	β (K min^{-1})				
NZPO	692.34	700.00	707.20	711.70	722.20
NZPO/1Cu	694.01	703.25	709.50	713.10	717.13
NZPO/5Cu	699.01	703.80	710.81	714.64	720.94

site within the crystalline phase without creating a new phase.

The DTA thermograms of NZPO, NZPO/1Cu and NZPO/5Cu glass samples, at different heating rates ranging from 15 to 35 K min^{-1}, are shown in Fig. 3.

The DTA curves for the amorphous NZPO glass sample reveal the presence of two successive endothermic peaks (i.e. T_e and T_g) and one last exothermic peak (i.e. T_c) as shown in Fig. 3a. These very small peaks with characteristic temperatures T_e and T_g are attributed to the release of adsorbed water from the surface of the solid and glass transition temperature, respectively. The peak with characteristic temperature T_c is ascribed to the crystallization of this glass. This result confirms that the NZPO sample has crystallized with $Na_2ZnP_2O_7$ structure as revealed by XRD results. The present DTA behavior of NZPO glass is in good agreement with previous studies [30,32,33]. In some earlier studies [32, 34], two crystallization peaks or asymmetric crystallization peaks were observed which is not the case for the present investigation. This may be associated with the presence of two amorphous phases, different crystallization mechanisms or distinct phase transformations.

The Cu-doped NZPO glass thermograms (Fig. 3b and 3c) show the presence of three additional (T_{g1}, T_{O1} and T_{O2}) peaks comparatively to non-doped ones. The T_e and T_{g1} points are associated with the evaporation of remaining water in the solid and the first glass transition temperatures, respectively. For the P_2O_5-V_2O_5-CuO glass system, two phase transitions were highlighted, the first one occurred around ~ 500 K in the sample that contained 2.5 mol% of CuO [35]. The exo-peaks T_{O1} and T_{O2} are related to the gradual oxidation of copper following the transformations, Cu → Cu_2O → CuO. In air atmosphere, the Cu_2O oxide can be formed by the oxidation of copper, followed by CuO formation as a final state during the heating process [36,37]. The Cu_2O can be formed below 473 K while the formation of CuO can be achieved above [37,38]. The second glass transition noted T_{g2} approximatively agrees with the T_g in the NZPO sample [30]. The crystallization of NZPO/1Cu and NZPO/5Cu samples is recognized by the last T_c exothermic peaks at different heating rates, and both crystallized as $Na_2ZnP_2O_7$ phase, as confirmed in Fig. 2. It is obvious that the characteristic behavior of DTA scans depends on the matrix chemical composition, preparation procedure and other factors.

One of the main objectives of this investigation was to study the crystallization kinetics as a function of the Cu content. Fig. 4 shows the normalized crystallization peaks for NZPO (Fig. 4a), NZPO/1Cu (Fig. 4b) and NZPO/5Cu (Fig. 4c) at different heating rates up to 35 min K^{-1}. Table 2 presents the characteristic temperatures T_c extracted from these curves. The crystallization peak temperatures are in the range of 692.3 – 722.2, 694.0 – 717.1 and 699.0 – 720.9 K for NZPO, NZPO/1Cu and NZPO/5Cu glass samples, respectively.

The crystallized fraction (X) at any temperature T can be calculated by evaluating the partial area under the crystallization peak and following the equation [39–41]:

$$X = \frac{A_T}{A} \tag{3}$$

where A_T is the area under the crystallization peak between the onset temperature and a given temperature T and A is the total area under the whole peak.

Figs. 5 and 6 show the evolution of the crystallized fraction (X) for both non-doped and Cu-doped samples as a function of temperature and

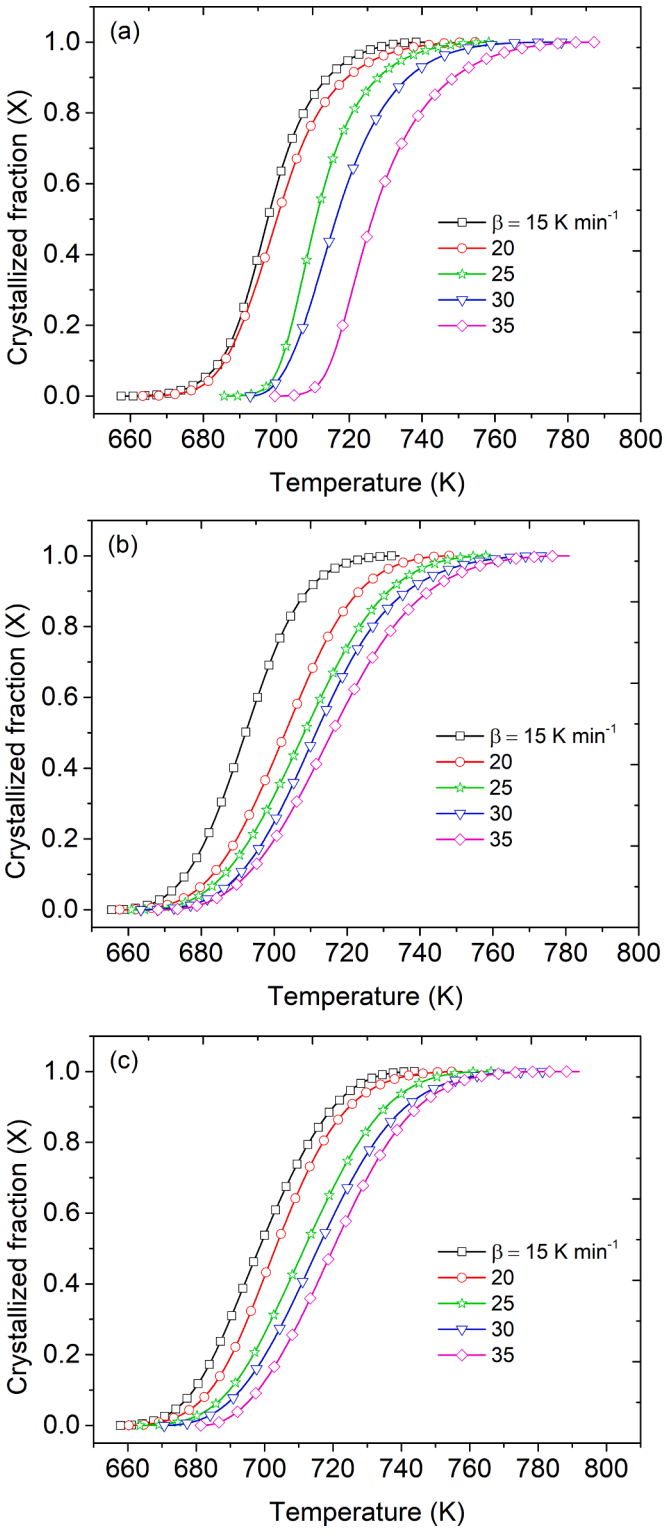

Fig. 5. Crystallized fraction curves vs. temperature of: (a) NZPO, (b) NZPO/1Cu and (c) NZPO/5Cu; glass samples.

normalized scanning time at various heating rates, respectively. It can be seen that the variation of the crystallized fraction with temperature and time has a sigmoid shape and X plot shifts towards high temperature with increasing heating rate. On the other hand, from Fig. 4, it can be observed that with increasing heating rate both the crystallization peak temperature for all the glass materials and the available amount of heat per unit time at higher heating rates increased [42]. These observations

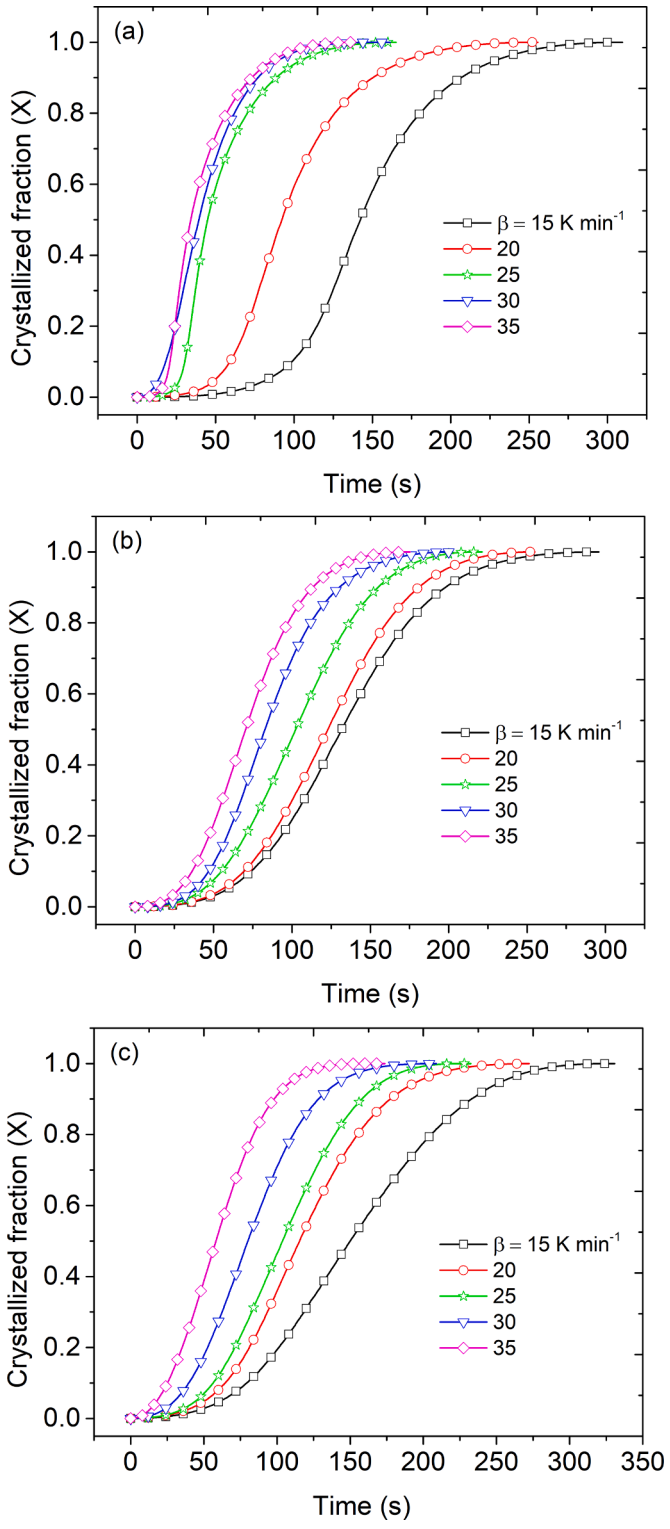

Fig. 6. Crystallized fraction as function of time for (a) NZPO, (b) NZPO/1Cu and (c) NZPO/5Cu, glass samples.

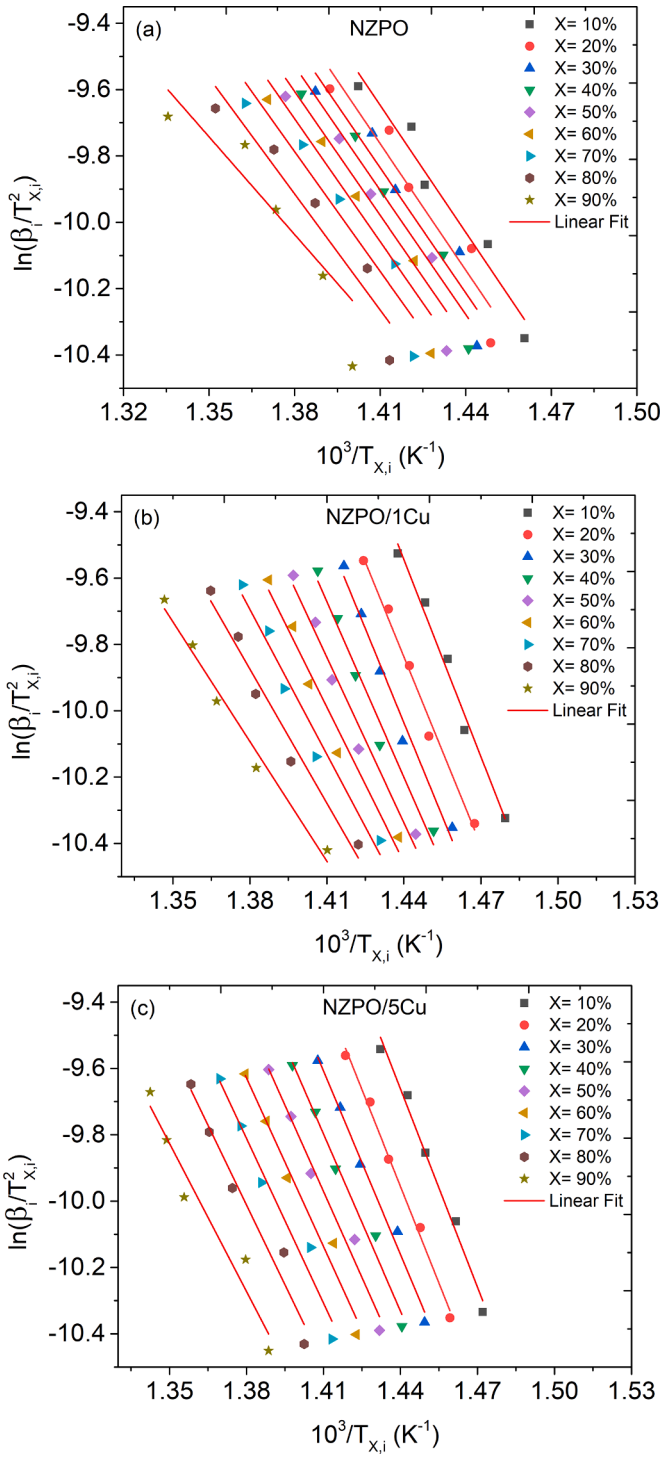

Fig. 7. KAS plots corresponding to the crystallization peak for (a) NZPO, (b) NZPO/1Cu and (c) NZPO/5Cu samples.

are in good agreement with previous findings [39–41,43], and confirm that the crystallization phenomenon is thermally activated and kinetically controlled. As observed from Table 2, the increase in the Cu content induces slight shifts in the T_c temperature to higher values except at higher heating rates. Therefore, introducing the Cu element into the NZPO glass matrix delays its crystallization. This behavior can be clarified by considering the structural role of this element in the glass.

3.2. Activation energies and thermodynamic parameters

Due to the changes in the nucleation and growth behaviors during any phase transition, the corresponding activation energies may change during the whole crystallization phenomenon [44]. The crystallization activation energy can be calculated at different crystallized fractions by using the Kissinger-Akahira-Sunose (KAS) analytical method as follows [45,46]:

Table 3
Crystallization energies characteristics E_{KAS} and $\Delta H^{\#}$ for different glasses at different X and β values.

Sample	X (%)	E_{KAS} (kJ mol^{-1})	$\Delta H^{\#}$ (kJ mol^{-1})					
			15 β (K min^{-1})	20	25	30	35	Average of $\Delta H^{\#}$ (kJ mol^{-1})
NZPO	10	106.00 ± 1.59	100.30	100.29	100.16	100.14	100.05	106.18 ± 1.59
	20	105.50 ± 2.19	99.76	99.75	99.64	99.61	99.52	99.64 ± 2.19
	30	104.42 ± 2.14	98.66	98.64	98.54	98.51	98.42	98.54 ± 2.14
	40	103.67 ± 1.75	97.88	97.87	97.77	97.73	97.65	97.77 ± 1.75
	50	103.42 ± 2.14	97.61	97.59	97.50	97.46	97.38	97.50 ± 2.14
	60	101.39 ± 2.07	96.76	96.74	96.65	96.60	96.52	96.64 ± 2.07
	70	100.10 ± 2.04	94.25	94.22	94.14	94.08	93.99	94.12 ± 2.04
	80	97.02 ± 1.94	91.13	91.10	91.02	90.96	90.87	91.00 ± 1.94
	90	81.47 ± 2.50	75.53	75.48	75.45	75.41	75.24	75.38 ± 2.50
NZPO/1Cu	10	160.53 ± 1.38	158.91	158.84	158.82	158.78	158.77	158.84 ± 1.38
	20	157.55 ± 1.17	151.88	151.81	151.78	151.75	151.72	151.80 ± 1.17
	30	155.63 ± 1.50	149.93	149.85	149.81	149.78	149.76	149.84 ± 1.50
	40	146.49 ± 1.54	140.76	140.67	140.63	140.61	140.57	140.67 ± 1.54
	50	138.01 ± 1.55	132.25	132.16	132.12	132.09	132.05	132.15 ± 1.55
	60	129.28 ± 1.56	123.49	123.40	123.35	123.32	123.28	123.39 ± 1.56
	70	121.13 ± 1.47	115.31	115.21	115.16	115.13	115.09	115.20 ± 1.47
	80	112.07 ± 1.28	106.22	106.11	106.05	106.02	105.97	106.10 ± 1.28
	90	100.01 ± 0.91	94.11	93.99	93.92	93.88	93.83	93.97 ± 0.91
NZPO/5Cu	10	161.61 ± 1.26	159.96	159.92	159.87	159.84	159.80	159.88 ± 1.26
	20	160.45 ± 0.86	155.75	155.70	155.65	155.62	155.58	155.67 ± 0.86
	30	157.14 ± 1.03	151.40	151.36	151.30	151.27	151.23	151.31 ± 1.03
	40	147.90 ± 1.17	142.12	142.08	142.02	141.99	141.95	142.04 ± 1.17
	50	143.91 ± 1.34	138.10	138.06	137.99	137.96	137.92	138.01 ± 1.34
	60	140.75 ± 1.55	134.90	134.87	134.79	134.75	134.72	134.81 ± 1.55
	70	137.59 ± 1.67	131.70	131.67	131.59	131.55	131.51	131.61 ± 1.67
	80	133.27 ± 1.78	127.34	127.30	127.22	127.18	127.14	127.24 ± 1.78
	90	123.62 ± 1.96	117.63	117.59	117.48	117.45	117.42	117.52 ± 1.96

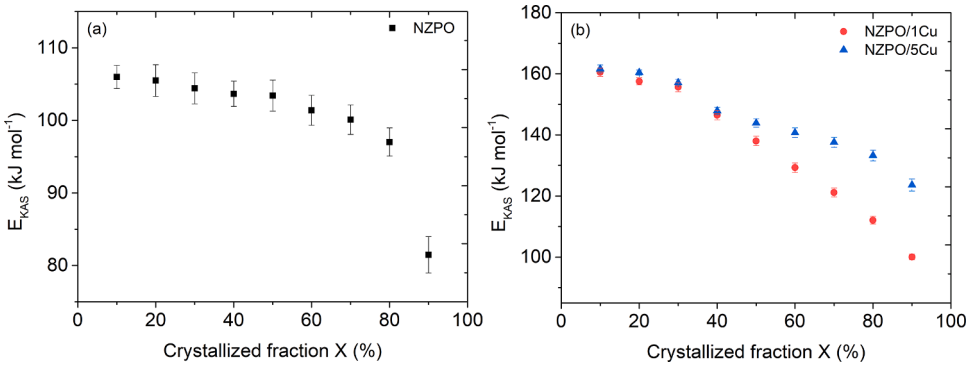

Fig. 8. Activation energy E_{KAS} vs. crystallized fraction X for (a) no-doped NZPO and (b) Cu-doped glass samples.

$$\ln\left(\frac{\beta_i}{T_{X,i}^2}\right) = -\frac{E_{KAS}}{RT_{X,i}} + C_K(X). \quad (4)$$

where E_{KAS} is the activation energy of phase transition, $T_{X,i}$ is the temperature at heating rate β_i and crystallized fraction X and $C_K(X)$ is a constant depending on X.

Fig. 7 shows the plots of $\ln(\beta_i/T_{X,i}^2)$ against $10^3/T_{X,i}$ for NZPO (Fig. 7a), NZPO/1Cu (Fig. 7b) and NZPO/5Cu (Fig. 7c) glass samples. The activation energies at different crystallized volume fractions could be estimated from the slopes of the KAS linear plots (i.e. lines in red color). The obtained activation energies versus the crystallization process degree for non-doped and Cu-doped samples are shown in Table 3 and presented in Fig. 8. It can be observed from Fig. 8, that the local activation energies reach more or less a steady state until ~ 50% crystallized fraction for NZPO and ~ 30% for Cu-doped samples then they decrease with increasing X values. This trend may be explained by the higher energy value corresponding to the onset of the nucleation process followed by both nucleation and growth. Subsequently, it is energy released during the growth of the crystalline phase until the final stage. This behavior has been observed and reported in previous studies for different glasses [16,30,31,47,48]. In addition, it is observed that doped samples show a convergence in energy range up to 40% followed by a clear divergence which may be explained by the fact that nucleation and growth characteristics were the same for both samples at this stage. The calculated values of E_{KAS} from $X = 90$ to 10% are in the range of 81.5 – 106.0, 100.0 – 160.5 and 123.6 – 161.6 kJ mol^{-1} for NZPO, NZPO/1Cu and NZPO/5Cu samples, respectively. Cu doped samples exhibit the highest values owing to their less susceptibility to crystallization and the fact that the crystallization process is delayed by the copper element.

Once the activation energies are calculated, the characteristic enthalpy $\Delta H^{\#}$ can be determined at different values of β and X (Table 3), using the following expression [49,50]:

$$\Delta H^{\#} = E_a - RT \quad (5)$$

where E_a corresponds to the energy E_{KAS}.

The enthalpy characteristic bears almost the same trend and value (~ - 3 kJ/mol) as E_{KAS}. The obtained average values decreased from 106.2 to 75.4 after 90% crystallized fraction for NZPO sample. NZPO/1Cu and NZPO/5Cu samples have the $\Delta H^{\#}$ values, 93.9 – 158.8 and 117.5 – 159.9 kJ mol^{-1}, respectively.

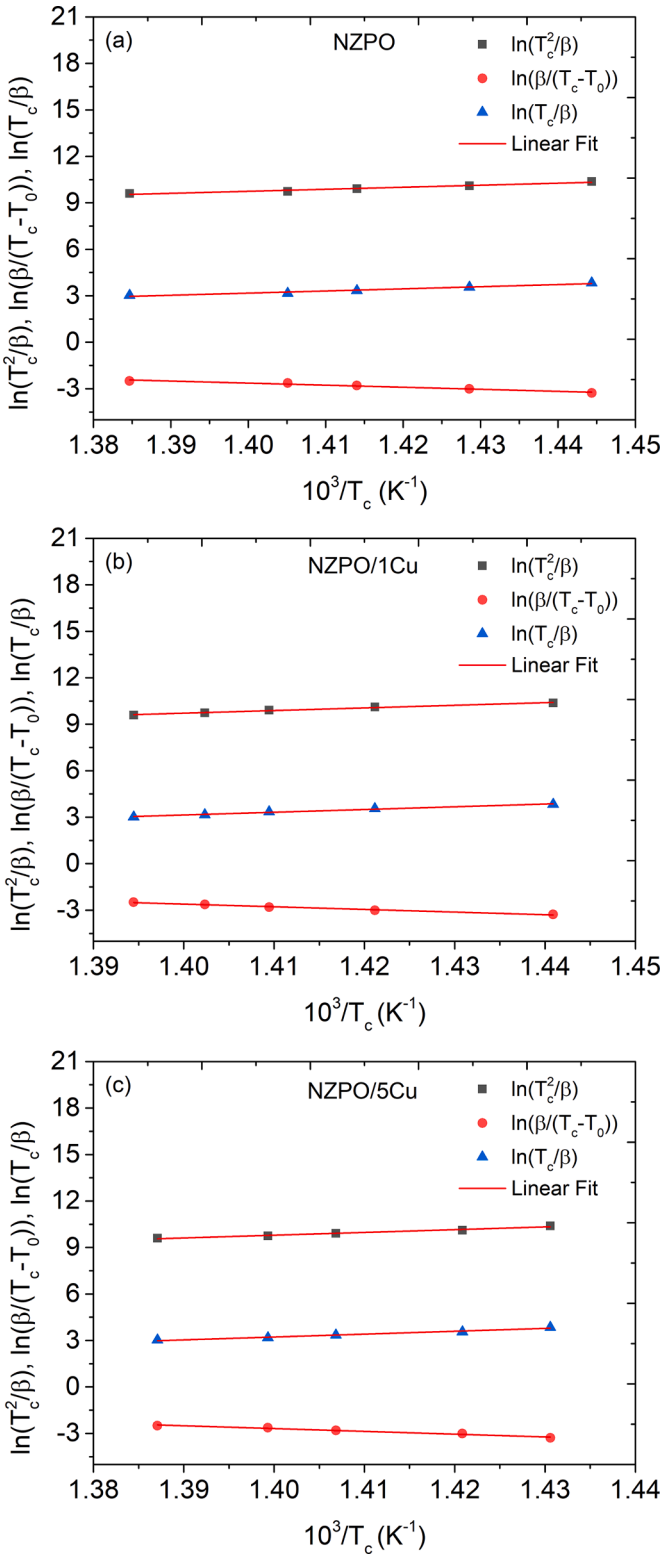

Fig. 9. Plots of $\ln(T_c^2/\beta)$, $\ln(\beta/(T_c - T_0))$ and $\ln(T_c/\beta)$ against $10^3/T_c$ for glass samples (a) NZPO, (b) NZPO/1Cu and (c) NZPO/5Cu.

To assess the activation energy at crystallization peak temperature T_c, three analytical methods were used, namely: Kissinger method [46], Augis–Bennett model (1) [51] and Augis–Bennett model (2) [52], given by Eqs. (6)–(8), respectively:

$$\ln\frac{T_c^2}{\beta} = \frac{E_{ck}}{RT_c} + \text{constant}. \tag{6}$$

$$\ln\frac{\beta}{(T_c - T_0)} = -\frac{E_{cab1}}{RT_c} + \ln(k_0). \tag{7}$$

$$\ln\frac{T_c}{\beta} = \frac{E_{cab2}}{RT_c} - \ln(\nu). \tag{8}$$

where E_{ck}, E_{cab1} and E_{cab2} are the activation energies calculated using the Kissinger and Augis-Bennett model (1) and (2), respectively; ν refers to the number of attempts made by the nuclei per second to overcome energy barrier for crystallization; k_0 represents the frequency or pre-exponential factor and T_0 is the starting DTA scan temperature.

Plots of $\ln(T_c^2/\beta)$, $\ln(\beta/(T_c - T_0))$ and $\ln(T_c/\beta)$ versus $10^3/T_c$ for all samples are shown in Fig. 9. Also, the deduced values of energies are shown in Table 4. As seen, the Kissinger and Augis-Bennett model (1) give closer values than the Augis-Bennett model (2), almost ~ 109, 141 and 149 kJ mol^{-1} for NZPO, NZPO/1Cu and NZPO/5Cu samples, respectively. It is clear that the energies E_{ck} and E_{cab1} are roughly close to those obtained using KAS method between ~ 40 and 50% in X for Cu-doped samples. E_{ck} and E_{cab1} values for non-doped sample are slightly higher than those presented in Table 3, where the E_{KAS} values exhibit a steady value around 104 kJ mol^{-1}, as discussed above.

The k_0 parameter can be derived from Eq. (7) and the obtained values are 6.78×10^7, 68.80×10^7 and 92.90×10^7 s^{-1} for NZPO, NZPO/1Cu and NZPO/5Cu glasses, respectively. The ν parameter values are calculated from Fig. 9 plots and are shown in Table 4. Information about the nucleation sites available for crystal growth can be obtained basing on ν trends. The resulting values of ν are 0.19×10^8, 1.31×10^{10} and 1.96×10^{10} s^{-1} for NZPO, NZPO/1Cu and NZPO/5Cu, respectively. The Cu-doped samples show higher values of ν as compared to the NZPO sample. This indicates that nuclei make maximum attempts per second to overcome the energy barrier, and at the same time, Cu^{2+}ions prevent this behavior, which leads to raising the characteristic energies of crystallization. In this case, Cu^{2+} ions may be responsible for a lower degree of depolymerization of the glass network. Previously, NZPO glass network containing Cu^{2+} ions depolymerized less than those doped with Co^{2+} and Ni^{2+} [31].

Since the activation energy and pre-exponential factor are calculated, the enthalpy of crystallization $\Delta H^{\#}$ at T_c can be easily determined using Eq. (5). For NZPO, NZPO/1Cu, and NZPO/5Cu glasses, the average enthalpy values are 102.2, 135.0, and 143.7 kJ mol^{-1}, respectively. Compared with Table 3, these values are in good agreement with those obtained at a crystallization range degree of ~ 40 − 50%.

The Gibbs free energy $\Delta G^{\#}$ and entropy of activation $\Delta S^{\#}$ can be calculated using the following equation [49,50]:

$$k_0 \exp\left(\frac{-E}{RT}\right) = \xi \exp\left(\frac{-\Delta G^{\#}}{RT}\right) \tag{9}$$

$$\Delta G^{\#} = \Delta H^{\#} - T\Delta S^{\#} \tag{10}$$

where $\xi = kT/h$, k and h are the Boltzman and Plank constants, respectively.

The computed thermodynamic parameters $\Delta G^{\#}$ and $\Delta S^{\#}$ are given in Table 4. For NZPO, NZPO/1Cu, and NZPO/5Cu samples, the average values of $\Delta G^{\#}$ and $\Delta S^{\#}$ are 180.2, 199.4, 206.7 kJ mol^{-1} and −110.5, −91.2, −88.7 J mol^{-1} respectively. Based on this data, the following conclusions can be drawn: The energies E, $\Delta H^{\#}$, $\Delta G^{\#}$ and $\Delta S^{\#}$ increase significantly for the Cu-doped samples comparatively to non-doped glass and this confirms that the Cu^{2+} ion has delayed the crystallization process. It was reported in previous work that the activation energy for the ion transport (ΔE_{dc}) increased with the addition of 5 mol% of copper amount in the glass to reach a value of about ~ 100 kJ mol^{-1}, as compared to 5 mol% (Co or Ni) co-doped-NZPO (~ 85.87 kJ mol^{-1}) and

Table 4
Various crystallization kinetics characteristics for different glass samples.

Sample		β (K min^{-1})					Average
		15	20	25	30	35	
NZPO	E_{ck} (kJ mol^{-1})	109.08 ± 1.63					
	E_{cab1} (kJ mol^{-1})	110.06 ± 1.62					
	E_{cab2} (kJ mol^{-1})	118.30 ± 1.63					
	$\nu\times 10^{8}$ (s^{-1})	0.19					
	$k_0\times 10^{7}$ (s^{-1})	6.78					
	$\Delta H^{\#}$ (kJ mol^{-1})	102.29	102.26	102.20	102.16	102.10	102.20 ± 1.63
	$\Delta G^{\#}$ (kJ mol^{-1})	179.12	179.42	180.32	180.82	181.54	180.24 ± 1.62
	$\Delta S^{\#}$ (J mol^{-1} K^{1})	−110.34	−110.37	−110.47	−110.52	−110.60	−110.46 ± 1.63
NZPO/1Cu	E_{ck} (kJ mol^{-1})	140.92 ± 1.12					
	E_{cab1} (kJ mol^{-1})	142.50 ± 1.12					
	E_{cab2} (kJ mol^{-1})	146.82 ± 1.12					
	$\nu\times 10^{10}$ (s^{-1})	1.31					
	$k_0\times 10^{7}$ (s^{-1})	68.80					
	$\Delta H^{\#}$ (kJ mol^{-1})	135.16	135.07	135.02	135.01	134.97	135.05 ± 1.14
	$\Delta G^{\#}$ (kJ mol^{-1})	198.17	199.13	199.66	199.82	200.26	199.41 ± 1.14
	$\Delta S^{\#}$ (J mol^{-1} K^{1})	−91.03	−91.15	−91.22	−91.24	−91.30	−91.19 ± 1.14
NZPO/5Cu	E_{ck} (kJ mol^{-1})	149.65 ± 1.53					
	E_{cab1} (kJ mol^{-1})	149.71 ± 1.53					
	E_{cab2} (kJ mol^{-1})	157.96 ± 1.53					
	$\nu\times 10^{10}$ (s^{-1})	1.96					
	$k_0\times 10^{7}$ (s^{-1})	92.90					
	$\Delta H^{\#}$ (kJ mol^{-1})	143.83	143.80	143.74	143.70	143.68	143.75 ± 2.12
	$\Delta G^{\#}$ (kJ mol^{-1})	205.77	206.17	206.83	207.17	207.46	206.68 ± 2.12
	$\Delta S^{\#}$ (J mol^{-1} K^{1})	−88.61	−88.67	−88.75	−88.80	−88.84	−88.73 ± 2.12

pure NZPO (∼ 91.66 kJ mol^{-1}) samples [31]. The lowest values of ΔE_{dc} and highest values of conductivity σ_{dc} reported in Co and Ni co-doped-NZPO were related to the higher mobility of Na^{+} ions in a disordered, weak and open phosphate structure resulting from the creation of non-bridging oxygen [31]. Therefore, the Cu-doped glass showed a stronger phosphate structure than pure, Co or Ni co-doped-NZPO glasses [31]. These results agree with the present finding about Cu delaying crystallization.

The obtained results of enthalpy in the present study for NZPO glass are close to that of $K_2ZnP_2O_7$ glass (103.47 kJ mol^{-1}) [53]. The negative value of $\Delta S^{\#}$ indicates that ions are more closely aligned in the activated state due to dipole-dipole interactions [53]. The ratio of $\Delta S^{\#}/k$ values are ∼ −13.3, −10.9 and −10.7 for NZPO, NZPO/1Cu, and NZPO/5Cu. $\Delta S^{\#}/k$ values were about ∼ −1.01, −1.05 and −0.35 for $LiNi_{1.5}P_2O_7$ [54], $K_2NiP_2O_7$ [20] and $K_2ZnP_2O_7$ [53] glasses, respectively. The lower ratio values are connected with the lower decomposition of $Na_2ZnP_2O_7$ than the $K_2(Zn/Ni)P_2O_7$ counterparts [55].

3.3. Avrami's exponent and numerical factor

The Avrami exponent n can be obtained from an exothermic peak by using the following modified Ozawa equation [56]:

$$\left|\frac{d[\ln(-\ln(1-X))]}{d\ ln\beta}\right|_T = -n \tag{11}$$

where X is the crystallized fraction at heating rate β and fixed temperature T.

Plots of ln[-ln(1-X)] against ln(β) at different fixed temperatures for NZPO, NZPO/1Cu and NZPO5/Cu are shown in Fig. 10. The values of n can be calculated from the slopes of Ozawa plots and are ∼ 3.11 and ∼ 2.04 for no doped and doped samples (Table 5).

Matusita and co-workers [57–59] have proposed a model (Eq. (12)) to calculate the m parameter which is known as numerical factor that depends on the crystal growth's dimensions characteristic.

$$\ln\left(\frac{\beta^n}{T_c^2}\right) = -\frac{mE_c}{RT_c} + \text{constant} \tag{12}$$

Fig. 11 shows the plots of $\ln(\beta^n/T_c^2)$ vs. $10^3/T_c$ for different glass samples. Straight lines are obtained and m values can be deduced from the slopes of plots. The values and trends for m are close to the n parameter in the present study, almost ∼ 3 and ∼ 2 for non-doped and Cu-doped NZPO glass samples, as shown in Table 5. From the tabulated values of n and m parameters (Table 6) [60], which summarizes the various reaction mechanisms, the crystallization processes were of three and two-dimensional growth of crystals for NZPO and both of doped samples, respectively, where the number of nuclei is independent of the heating rate (i.e. constant number of nuclei). According to the roughly constant obtained characteristic energies (See Tables 3 and 4) at various β values for each sample, the concluded process mechanisms are confirmed. Moreover, the convergence observed in activation energy E_{KAS} for doped samples up to 50% in X is consistent with the same crystallization mechanism. The difference in dimensional growth of crystals may be ascribed to the change in structural units caused by the Cu element in the glass matrix, as discussed above.

4. Conclusion

Thermal and structural analysis of diphosphate glasses with chemical composition $Na_2Cu_xZn_{1-x}P_2O_7$ (x = 0, 1 and 5 mol%) were carried out, using X-ray diffraction and differential thermal analysis. All the glasses have been crystallized with a tetragonal structure $Na_2ZnP_2O_7$ (PDF 01–087–0499). The combination of several analytical methods led us to a better understanding the effect of copper oxide addition on the crystallization kinetics in the present glass system. Thermodynamic parameters such as activation energy E_c, enthalpy $\Delta H^{\#}$, Gibbs free energy $\Delta G^{\#}$ and entropy $\Delta S^{\#}$, are calculated. The activation energies increase with the introduction of copper element into the glass network. Moreover, calculated morphological parameters n and m show that the present glasses are mainly controlled by bulk crystallization mechanism with a constant number of nuclei. Crystal growths are three and two-dimensional for no doped and copper co-doped NZPO compositions. On the other hand, the values of ν and k_0 parameters increase with Cu addition. Finally, the DTA results revealed that the peak temperatures and activation energies of the crystallization process increase with copper doping. Thus, the addition of Cu element into the NZPO glass matrix delays its crystallization and acts as a structural modifier.

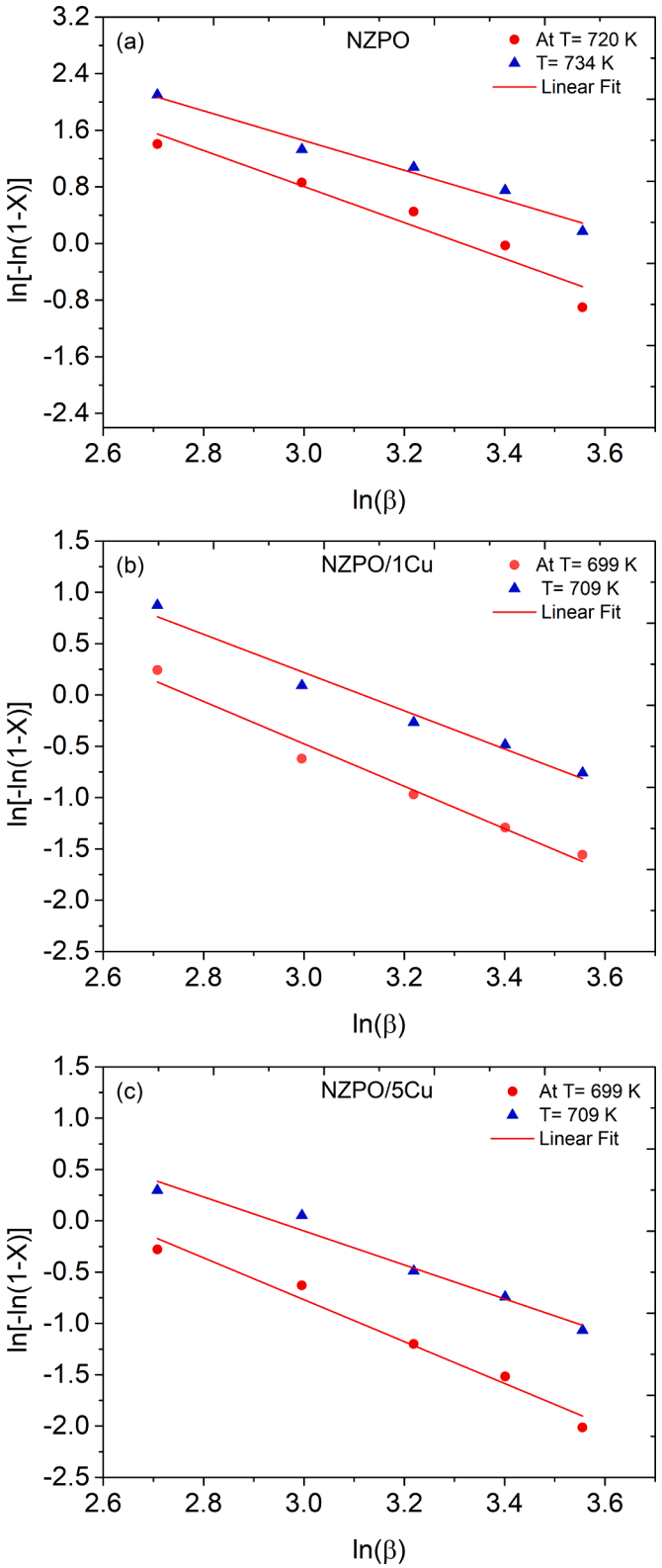

Fig. 10. Plot of ln[-ln(1-X)] vs. ln(β) for non-doped and Cu-doped glass samples.

CRediT authorship contribution statement

Majda Khaldi: Data curation, Investigation. **Yousf Islem Bourezg:** Data curation, Methodology, Writing – original draft, Writing – review & editing. **Mohamed Kharroubi:** Supervision, Writing – original draft, Writing – review & editing. **Foudil Sahnoune:** Investigation. **Messaoud Harfouche:** Writing – original draft. **Ahcen Keziz:** Investigation. **Mostafa Maache:** Visualization. **Lakhdar Gacem:** Conceptualization. **Djamel Bradai:** Writing – original draft.

Table 5
Avrami and numerical factor parameters obtained in the present study.

Parameter	Sample		
	NZPO	NZPO/1Cu	NZPO/5Cu
n	3.11	2.06	2.04
m	3.25	2.00	1.94

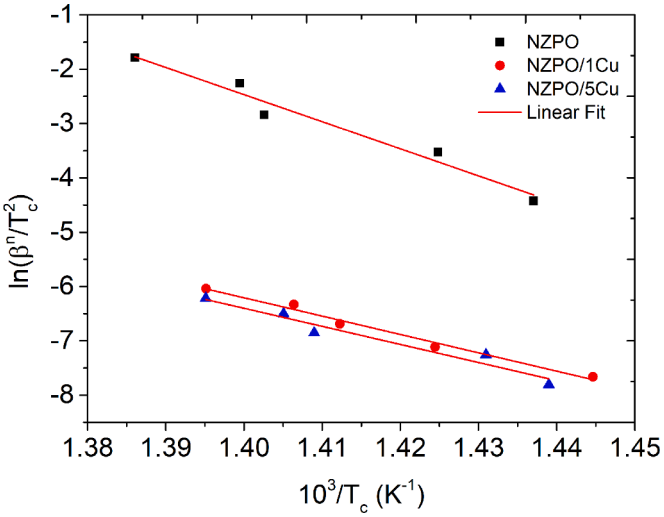

Fig. 11. Matusita-Sakka plots for non-doped and Cu-doped glass samples.

Table 6
Different crystallization mechanisms in the heating process [60].

Crystallization mechanism	Avrami exponent, n	Numerical factor, m
Bulk crystallization with a constant number of nuclei (i.e. the number of nuclei is independent of the heating rate)		
Three-dimensional growth of crystals	3	3
Two-dimensional growth of crystals	2	2
One-dimensional growth of crystals	1	1
Bulk crystallization with an increasing number of nuclei (i.e. the number of nuclei is inversely proportional to the heating rate)		
Three-dimensional growth of crystals	4	3
Two-dimensional growth of crystals	3	2
One-dimensional growth of crystals	2	1
Surface crystallization	1	1

Declaration of competing interest

The authors declare that they have no known competing financial interests or personal relationships that could have appeared to influence the work reported in this paper.

Data availability

Data will be made available on request.

Acknowledgement

PRFU national project under Grant Agreement No. B00L02UN170120220001, was funded by DGRSDT under the Directorate General for Scientific Research and Technological Development (DGRSDT).

References

[1] J. Miroslav, P. Znášik, D. Tunega, M.D. Ingram, Glass formation and structure in the system $Cu_2OP_2O_5MoO_3$, J. Non-Cryst. Solids 185 (1995) 151–158, https://doi.org/10.1016/0022-3093(94)00642-3.

[2] R.C. Nageswara, P.V. Rao, R. Kameswari, R.R. Raju, G. Chandana, K. Samatha, MVVK.S. Prasad, M. Venkateswarlu, A. Naveen, G.G. Dhar, Luminescence investigations on Dy^{3+} doped CdO-PbF_2 phosphate glass-ceramics, J. Mol. Struct. 1243 (2021) 130784, https://doi.org/10.1016/j.molstruc.2021.130784.

[3] W. Fu, L. Li, H. Zhu, Q. Liao, J. Zeng, Y. Wang, K. Wu, Y. Zhu, Effects of heat treatment temperature and CeO_2 content on the phase composition, structure, and properties of monazite phosphate-based glass-ceramics, J. Non-Cryst. Solids 588 (2022) 121631, https://doi.org/10.1016/j.jnoncrysol.2022.121631.

[4] F. Hiroshi, H. Matsunaga, S. Yamanaka, Crystal structure and ionic conductivity of ruthenium diphosphate $ARu_2(P_2O_7)_2$, A= Li, Na, and Ag, with a tunnel structure, Mater. Res. Bull. 38 (2003) 991–1001, https://doi.org/10.1016/S0025-5408(03)00067-9.

[5] A.C. Joshi, M. Roy, D.P. Dutta, R.K. Mishra, S.S. Meena, R. Kumar, D. Bhattacharyya, R. Alexander, C.P. Kaushik, A.K. Tyagi, Effect on the structure and stability of iron phosphate glass with Sb and Te-ion loading for nuclear waste storage application, J. Non-Cryst. Solids 570 (2021) 121016, https://doi.org/10.1016/j.jnoncrysol.2021.121016.

[6] N. Shin-ichi, M. Nakamura, R. Natsui, A. Yamada, New lithium iron pyrophosphate as 3.5V class cathode material for lithium ion battery, J. Am. Chem. Soc. 132 (2010) 13596–13597, https://doi.org/10.1021/ja106297a.

[7] W. Shiquan, X. Jiang, G. Du, Z. Guo, J. Jang, S.J. Kim, Solvothermal synthesis of $Mn_2P_2O_7$ and its application in lithium-ion battery, Mater. Lett. 65 (2011) 3265–3268, https://doi.org/10.1016/j.matlet.2011.07.027.

[8] M. Llusar, A. García, C. Gargori, R. Galindo, J.A. Badenes, G. Monrós, Synthesis of diphosphate $Mn_{2-x}Mg_xP_2O_7$ solid solutions with thortveitite structure: new pink ceramic dyes for the colouration of ceramic glazes, J. Eur. Ceram. Soc. 32 (2012) 765–776, https://doi.org/10.1016/j.jeurceramsoc.2011.10.051.

[9] T. Cristina, M. Ricci, C. Ferrara, G. Bruni, V. Berbenni, E. Quartarone, P. Mustarell, Glucose-assisted synthesis and wet-chemistry preparation of pyrophosphate cathodes for rechargeable Na-ion batteries, RSC Adv. 6 (2016) 99735–99742, https://doi.org/10.1039/C6RA21919E.

[10] K. Heejin, R.A. Shakoor, C. Park, S.Y. Lim, J.S. Kim, Y.N. Jo, W. Cho, K. Miyasaka, R. Kahraman, Y. Jung, J.W. Choi, $Na_2FeP_2O_7$ as a promising iron-based pyrophosphate cathode for sodium rechargeable batteries: a combined experimental and theoretical study, Adv. Funct. Mater. 23 (2013) 1147–1155, https://doi.org/10.1002/adfm.201201589.

[11] E. Fatima, A. Boukhari, F. Abraham, B. Elouadi, The crystal structure of α-and β-$Na_2CuP_2O_7$, J. Solid State Chem. 120 (1995) 23–31, https://doi.org/10.1006/jssc.1995.1370.

[12] B. Prabeer, J. Lu, T. Ye, M. Kajiyama, S.C. Chung, N. Yabuuchi, S. Komaba, A. Yamada, A layer-structured $Na_2CoP_2O_7$ pyrophosphate cathode for sodium-ion batteries, RSC Adv. 3 (2013) 3857–3860, https://doi.org/10.1039/C3RA23026K.

[13] N. Shin-ichi, M. Nakamura, R. Natsui, A. Yamada, New lithium iron pyrophosphate as 3.5 V class cathode material for lithium ion battery, J. Am. Chem. Soc. 132 (2010) 13596–13597, https://doi.org/10.1021/ja106297a.

[14] A. Semih, F. Krumeich, C. Mensing, A. Borgschulte, R. Nesper, New high capacity cathode materials for rechargeable Li-ion batteries: vanadate-borate glasses, Sci. Rep. 4 (2014) 7113, https://doi.org/10.1038/srep07113.

[15] M. Farouk, K. Abdallauh, M. Attallah, Z.M. Abd El-Fattah, Influence of different alkaline oxide modifiers on VO^{2+} ions doped zinc borate glasses, J. Non-Cryst. Solids 523 (2019) 119607, https://doi.org/10.1016/j.jnoncrysol.2019.119607.

[16] A. Hamza, M. Kharroubi, Dielectric studies and Cole-Cole plot analysis of Na_2O–(1-x)ZnO–xCoO–P_2O_5 glasses, J. Non-Cryst. Solids 560 (2021) 120721, https://doi.org/10.1016/j.jnoncrysol.2021.120721.

[17] I. Belharouak, P. Gravereau, C. Parent, J.P. Chaminade, E. Lebraud, G. Le Flem, Crystal structure of $Na_2ZnP_2O_7$: reinvestigation, J. Solid State Chem. 152 (2000) 466–473, https://doi.org/10.1006/jssc.2000.8714.

[18] Y.F. Shepelev, M.A. Petrova, A.S. Novikova, A.E. Lapshin, Crystal structures of $Na_2ZnP_2O_7$, $K_2ZnP_2O_7$, and $LiKZnP_2O_7$ phases in the M_2O–ZnO–P_2O_5 glass-forming system (M= Li, Na, and K), Glass Phys. Chem. (2002) 317–321, https://doi.org/10.1023/A:1020752811708.

[19] R. Ben Said, B. Louati, K. Guidara, AC conduction mechanism of the zinc potassium diphosphate, Ionics 23 (2017) 2397–2404, https://doi.org/10.1007/s11581-017-2070-5.

[20] R. Ben Said, B. Louati, K. Guidara, Electrical conduction and thermodynamic properties of $K_2NiP_2O_7$, Ionics 20 (2014) 209–219, https://doi.org/10.1007/s11581-013-0978-y.

[21] R. Belbal, L. Gacem, B. Bentria, H.A. Ahsaine, M.T. Soltani, B. Saidat, E.A. Ghezal, A. Gueddim, L. Guerbous, Synthesis and luminescence spectroscopy study of a novel orange-red colour emissions phosphor based on Tb^{3+} ion-doped $Na_2ZnP_2O_7$, Luminescence 36 (2021) 489–496, https://doi.org/10.1002/bio.3968.

[22] S.H. Jo, H. Yoon, B. Ju, D.W. Kim, Sodium-nickel pyrophosphate as a novel oxygen evolution electrocatalyst in alkaline medium, J. Am. Ceram. Soc. 103 (2020) 4748–4753, https://doi.org/10.1111/jace.17195.

[23] T. Cristina, M. Ricci, C. Ferrara, G. Bruni, E. Quartarone, P. Mustarelli, Electrochemical study of $Na_2Fe_{1-x}Mn_xP_2O_7$ (x = 0, 0.25, 0.5, 0.75, 1) as cathode material for rechargeable Na-ion batteries, Batteries 2 (2016) 1, https://doi.org/10.3390/batteries2010001.

[24] B. Prabeer, G. Liu, Z. Mohamed, C.D. Ling, A. Yamada, Structural, magnetic and electrochemical investigation of novel binary $Na_{2-x}(Fe_{1-y}Mn_y)P_2O_7$ ($0 \le y \le 1$) pyrophosphate compounds for rechargeable sodium-ion batteries, Solid State Ion. 268 (2014) 305–311, https://doi.org/10.1016/j.ssi.2014.03.011.

[25] C. Ferrara, C. Ritter, P. Mustarelli, C. Tealdi, Polymorphism in $Na_2(Co/Zn)P_2O_7$ and $Na_2(Co/Fe)P_2O_7$ pyrophosphates: a combined diffraction and 31P NMR study, J. Phys. Chem. C 126 (2021) 701–708, https://doi.org/10.1021/acs.jpcc.1c08753.

[26] R. Marzouki, A. Guesmi, M.F. Zid, A. Driss, Synthesis, crystal structure and electrical properties of a new mixed compound $(Na_{0.71}Ag_{0.29})_2CoP_2O_7$, Cryst. Struct. Theory appl. 1 (2012) 68, https://doi.org/10.4236/csta.2012.13013.

[27] R.O. Omrani, S. Krimi, J.J. Videau, I. Khattech, A. El Jazouli, M. Jemal, Structural investigations and calorimetric dissolution of manganese phosphate glasses, J. Non-Cryst. Solids 389 (2014) 66–71, https://doi.org/10.1016/j.jnoncrysol.2014.02.006.

[28] R.O. Omrani, S. Krimi, J.J. Videau, I. Khattech, A. El Jazouli, M. Jemal, Structural and thermochemical study of Na_2O–ZnO–P_2O_5 glasses, J. Non-Cryst. Solids 390 (2014) 5–12, https://doi.org/10.1016/j.jnoncrysol.2014.02.020.

[29] R.O. Omrani, A. Kaoutar, A. El Jazouli, S. Krimi, I. Khattech, M. Jemal, J.J. Videau, M. Couzi, Structural and thermochemical properties of sodium magnesium phosphate glasses, J. Alloys Compd. 632 (2015) 766–771, https://doi.org/10.1016/j.jallcom.2015.01.297.

[30] H. Ramdani, Y.I. Bourezg, M. Kharroubi, F. Sahnoune, L. Gacem, Investigation of crystallization kinetics of $Na_2ZnP_2O_7$ glass using XRD and DTA analysis, Cryst. Res. Technol. (2023) 2200257, https://doi.org/10.1002/crat.202200257.

[31] C. Kalai, M. Kharroubi, L. Gacem, S. Balme, A. Belbel, F. Lalam, Effect of transition-metal ions (Ni^{2+}, Cu^{2+} and Co^{2+}) on the electric and dielectric properties of zinc sodium phosphate, Glass Phys. Chem. 45 (2019) 503–512, https://doi.org/10.1134/S1087659619060087.

[32] E.R. Shaaban, Y.B. Saddeek, M. Abdel Rafea, Crystallization kinetics of the TeO2–BaO glass system, Philos. Mag. 89 (2009) 27–39, https://doi.org/10.1080/14786430802566406.

[33] J.X. Xiaojie, C.S. Ray, D.E. Day, Nucleation and crystallization of $Na_2O{\cdot}2CaO{\cdot}3SiO_2$ glass by differential thermal analysis, J. Am. Ceram. Soc. 74 (1991) 909–914, https://doi.org/10.1111/j.1151-2916.1991.tb04321.x.

[34] V.C.S. Reynoso, K. Yukimitu, T. Nagami, C.L. Carvalho, J.C.S. Moraes, E.B. Araujo, Crystallization kinetics in phosphate sodium-based glass studied by DSC technique, J. Phys. Chem. Solids 64 (2003) 27–30, https://doi.org/10.1016/S0022-3697(02)00204-4.

[35] A.A. Kutub, F.H. Al-Ghorabie, S.S. Natto, A.M. Alsanoosi, S.S. Babkair, A.S. Faidah, Spectroscopic and DSC studies of vanadium-copper-phosphate glasses, J. Mater. Sci. 27 (1992) 1343–1346, https://doi.org/10.1007/BF01142050.

[36] M. Bjoern, N. Nilius, Oxidation of polycrystalline copper films–pressure and temperature dependence, Thin Solid Films 651 (2018) 24–30, https://doi.org/10.1016/j.tsf.2018.02.007.

[37] L. Jindřich, D. Sedmidubský, M. Lojka, O. Jankovský, The effect of nanosizing on the oxidation of partially oxidized copper nanoparticles, Materials 13 (2020) 2878, https://doi.org/10.3390/ma13122878.

[38] Y. Akihiro, S. Tanaka, Oxidation behavior of copper nanoparticles at low temperature, Mater. Res. Bull. 46 (2011) 2323–2327, https://doi.org/10.1016/j.materresbull.2011.08.043.

[39] Y.I. Bourezg, H. Azzeddine, K. Abib, Y. Huang, D. Bradai, T.G. Langdon, Recrystallization in an Mg-Nd alloy processed by high-pressure torsion: a calorimetric analysis, J. Mater. Res. Technol. 9 (2020) 3047–3054, https://doi.org/10.1016/j.jmrt.2020.01.035.

[40] Y.I. Bourezg, D. Elfiad, H. Azzeddine, D. Bradai, Investigation of recrystallization kinetics in hot-rolled Mg-La alloy using differential scanning calorimetry technique, Thermochim. Acta 690 (2020) 178688, https://doi.org/10.1016/j.tca.2020.178688.

[41] Y.I. Bourezg, K. Abib, H. Azzeddine, D. Bradai, Kinetics of Cr clustering in a Cu-Cr-Zr alloy processed by equal-channel angular pressing: a DSC study, Thermochim. Acta 686 (2020) 178550, https://doi.org/10.1016/j.tca.2020.178550.

[42] S.R. Joshi, A. Pratap, N.S. Saxena, M.P. Saksena, A. Kumar, Heating rate and composition dependence of the glass transition temperature of a ternary chalcogenide glass, J. Mater. Sci. Lett. 13 (1994) 77–79, https://doi.org/10.1007/BF00416803.

[43] T. Sahraoui, F. Chouia, Y.I. Bourezg, A. Guelil, Effect of natural phosphate content on the growth kinetics of hydroxyapatite crystals grown from kaolin clay, Mater. Chem. Phys. 292 (2022) 126865, https://doi.org/10.1016/j.matchemphys.2022.126865.

[44] M. Koushik, K.B.R. Varma, Crystallization kinetic studies of $CaBi_2B_2O_7$ glasses by non-isothermal methods, J. Mater. Sci. 44 (2009) 385–391, https://doi.org/10.1007/s10853-008-3149-1.

[45] H.E. Kissinger, Reaction kinetics in differential thermal analysis, Anal. Chem. 29 (1957) 1702–1706, https://doi.org/10.1021/ac60131a045.

[46] H.E. Kissinger, Differential thermal analysis, J. Res. Natl. Bur. Stand. 57 (1956) 217.

[47] Y.C. Tang, G.T. Ma, N. Nollmann, G. Wilde, M. Zeng, C.H. Hu, L. Li, C. Tang, Comparative study of thermal stability and crystallization kinetics between melt-spun and bulk $Pd_{77.5}Cu_6Si_{16.5}$ metallic glasses, J. Mater. Res. Technol. 17 (2022) 2203–2219, https://doi.org/10.1016/j.jmrt.2022.01.147.

[48] L.K. Zhang, Z.H. Chen, Q. Zheng, D. Chen, Isochronal and isothermal phase transformation of $Cu_{45}Zr_{45}Ag_7Al_3$ bulk metallic glass, Phys. B 411 (2013) 149–153, https://doi.org/10.1016/j.physb.2012.12.001.

[49] P. Petr, T. Opravil, F. Šoukal, Introduction of novel kinetic approach to calculation of activation energy and its application to the sinter-crystallization of strontian feldspar, Ceram. Int. 42 (2016) 16969–16980, https://doi.org/10.1016/j.ceramint.2016.07.203.

[50] S.M. Pourmortazavi, I. Kohsari, M.B. Teimouri, S.S. Hajimirsadeghi, Thermal behaviour kinetic study of dihydroglyoxime and dichloroglyoxime, Mater. Lett. 61 (2007) 4670–4673, https://doi.org/10.1016/j.matlet.2007.03.041.
[51] J.A. Augis, J.E. Bennett, Calculation of the Avrami parameters for heterogeneous solid state reactions using a modification of the Kissinger method, J. Therm. Anal. 13 (1978) 283–292, https://doi.org/10.1007/BF01912301.
[52] H. Yinnon, D.R. Uhlmann, Applications of thermoanalytical techniques to the study of crystallization kinetics in glass-forming liquids, part I: theory, J. Non-Cryst. Solids 54 (1983) 253–275, https://doi.org/10.1016/0022-3093(83)90069-8.
[53] A.V. Sarode, A.C. Kumbharkhane, Dielectric relaxation study of poly (ethylene glycols) using TDR technique, J. Mol. Liq. 164 (2011) 226–232, https://doi.org/10.1016/j.molliq.2011.09.020.
[54] R. Ben Said, B. Louati, K. Guidara, S. Kamoun, Thermodynamic properties and application of CBH model in the ac conductivity of $LiNi_{1.5}P_2O_7$ ceramic, Ionics 20 (2014) 1071–1078, https://doi.org/10.1007/s11581-013-1060-5.
[55] A.A. Frost, R.G. Pearson, Kinetics and Mechanism, Wiley, New York, 1961.
[56] A.B. Selçuk, H. Yavuz, Gamma-irradiation effect on kinetic parameters of glass-ceramic materials, Mater. Lett. 57 (2003) 4382–4387, https://doi.org/10.1016/S0167-577X(03)00329-X.
[57] K. Matusita, S. Sakka, Y. Matsui, Determination of the activation energy for crystal growth by differential thermal analysis, J. Mater. Sci. 10 (1975) 961–966, https://doi.org/10.1007/BF00823212.
[58] K. Matusita, S. Sakka, Kinetic study of the crystallisation of glass by differential scanning calorimetry, Phys. Chem. Glas. 20 (1979) 81–84.
[59] M. Kazumasa, S. Sakka, Kinetic study of crystallization of glass by differential thermal analysis–criterion on application of Kissinger plot, J. Non-Cryst. Solids 38 (1980) 741–746, https://doi.org/10.1016/0022-3093(80)90525-6.
[60] H.C. Park, S.H. Lee, B.K. Ryu, M.M. Son, H.S. Lee, I. Yasui, Nucleation and crystallization kinetics of $CaO\text{-}Al_2O_3\text{-}2SiO_2$ in powdered anorthite glass, J. Mater. Sci. 31 (1996) 4249–4253, https://doi.org/10.1007/BF00356446.